electronics

MDPI

Article

Sine-Wave Filter Design Method for High-Speed PMSMs in High-Frequency (250 Hz) Drives

Genmao Zhou [1], Yinquan Ding [1], Zhennan Du [2], Yiwei Tang [1], Li Chen [1], Guohui Yang [1] and Gang Zhang [2,*]

[1] Xinjiang CNNC Tianshan Uranium Industry Co., Ltd., Ili 835300, China; zhougenmao@zhxjky.cn (G.Z.); dingyinquan@zhxjky.cn (Y.D.); tangyiwei@zhxjky.cn (Y.T.); chenli@zhxjky.cn (L.C.); yangguohui@zhxjky.cn (G.Y.)

[2] School of Electrical Engineering and Automation, Harbin Institute of Technology, Harbin 150001, China; 2022111845@stu.hit.edu.cn

* Correspondence: zhang_hit@hit.edu.cn

Abstract

In industrial applications such as in situ leaching and uranium mining, permanent magnet synchronous motors (PMSMs) for submersible pumps are frequently connected to frequency converters via long cables. During this long-distance transmission, traveling wave reflections induced by high-frequency pulse width modulation (PWM) generate severe transient overvoltages that threaten motor insulation. Because installation space at deep-well motor terminals is severely restricted, overvoltage suppression must be implemented at the inverter output. Here, the parameter design and optimization of a passive LC filter specifically developed for 250 Hz high-frequency PMSMs are presented. The optimal inductance and capacitance parameters were determined by balancing multiple operational constraints, including fundamental voltage drop, high-frequency harmonic attenuation, and the avoidance of low-order harmonic resonance. Furthermore, the anti-saturation performance of the magnetic core material, evaluated thermal characteristics through electromagnetic-thermal co-simulation, and analyzed the risk of self-excited oscillation between the filter capacitors and the motor was analyzed. Finally, hardware experiments conducted on a 20 m cable test bench validate that the designed LC filter effectively mitigates terminal overvoltage. The peak terminal voltage was reduced from 900 V to 505 V, and total harmonic distortion (THD) was limited to below 5%. This design provides a highly reliable, space-efficient solution for overvoltage suppression in high-speed, long-cable motor drive systems.

Keywords: variable frequency drive; overvoltage suppression; LC filter; permanent magnet synchronous motor; parameter design

Check for updates

Academic Editor: Raffaele Solimene

Received: 15 May 2026
Revised: 4 June 2026
Accepted: 9 June 2026
Published: 10 June 2026

Copyright: © 2026 by the authors. Licensee MDPI, Basel, Switzerland. This article is an open access article distributed under the terms and conditions of the Creative Commons Attribution (CC BY) license.

1. Introduction

In modern industrial automation, AC variable frequency speed regulation is widely utilized in applications such as fans, water pumps, compressors, and mine hoists. Despite its superior control performance, this technology introduces critical electrical challenges [1,2]. When the frequency drive and the motor are physically separated, long connecting cables are essential [3–5]. Because the PWM voltage generated by the drive features a high dv/dt and a steep rising edge, its transmission over long cables induces repeated traveling wave reflections. These waves superimpose at the motor terminals, generating overvoltage spikes that can reach nearly twice the DC bus voltage [6,7]. Such high-frequency, high-amplitude overvoltages accelerate the aging of motor stator insulation and risk catastrophic breakdown, fundamentally threatening system reliability [8].

To avoid the adverse impacts of motor terminal overvoltage on system reliability, equipment service life and operational stability, various suppression strategies have been proposed [6,9]. Current mainstream technologies are broadly categorized into active and passive filtering. Active power filters can flexibly suppress harmonics and overvoltages; however, they require complex control architectures and incur high costs. Furthermore, their reliability often degrades in harsh environments, limiting their deployment in scenarios like underground mining. Consequently, passive filters—characterized by their simple structure, high reliability, and cost-effectiveness—remain the preferred solution for industrial engineering [10].

Specifically, filters installed at the inverter output can effectively extend the pulse rise time and attenuate traveling wave reflections at the source. This configuration is particularly advantageous for deep-well submersible pumps, where installation space at the motor terminal is strictly constrained. Passive filter topologies primarily include RC, RLC, and LC configurations. As shown in Table 1, RC filters offer low cost and small size but suffer from poor frequency characteristics and power loss, making them inadequate for high-power and high-frequency applications [10]. RLC filters have excellent filtering characteristics and no significant resonance peaks [6,11], but they are bulky, heavy, costly, have significant additional losses, and involve complex design processes. By contrast, LC passive filters offer favorable frequency characteristics without introducing additional thermal losses [12,13].

Table 1. Topologies of Different Passive Filters.

Topology	Advantages	Limitations
RC Filter	Simple structure, low cost, small size	Poor frequency characteristics
LC Filter	Excellent frequency characteristics, high-power adaptability	Resonant peak exists, large volume and heavy weight
RLC Filter	Excellent frequency characteristics, no resonant peak	Large volume, heavy weight, high cost, obvious power loss and complex design

However, compared to RLC and RC configurations, LC filters possess a distinct structural drawback, namely the presence of an inherent, zero-damping resonance peak. If the filter parameters are improperly selected, the localized impedance minimum can severely amplify the low-order characteristic harmonics embedded within the PWM voltage spectrum. This amplification potentially triggers systemic electrical resonance, leading to severe waveform distortion, overcurrent tripping, and aggravated acoustic noise. While sensorless active damping techniques—such as virtual resistance insertion via state observers—can actively suppress such resonance, these control schemes demand high-bandwidth processors, exhibit heavy reliance on accurate motor parameters, and introduce significant algorithmic complexity, rendering them unviable for widespread, cost-sensitive industrial deployment [14–16]. Consequently, it is highly desirable to preemptively institutionalize this resonance constraint as an explicit boundary directly during the hardware parameter design phase. More importantly, conventional filter designs are optimized for low-frequency operating conditions (below 120 Hz). The theoretical framework and parameter optimization for high-frequency conditions (above 120 Hz)—where non-linear magnetic core losses (such as hysteresis and eddy current losses) escalate dramatically and high-order harmonics become distinctly problematic—remain underexplored.

To address this gap, this study investigates overvoltage suppression for a 250 Hz high-speed PMSM utilized in a submersible mining pump. We propose an inverter-side

passive LC overvoltage suppression device and detail a comprehensive parameter design methodology governed by multi-variable coupled boundaries. Distinct from conventional standalone parametric selection, this design methodology systematically integrates three closely interacted core dimensions tailored for high-frequency long-cable PMSM drives:

1. Parameter Feasible Region Design Considering High-Frequency Voltage Drop: Compared with conventional low-frequency (50/60 Hz) operations, the fundamental impedance of the filter inductor increases linearly at 250 Hz high-frequency operation, making the fundamental voltage drop significantly more severe and dominant. By analytically modeling this high-frequency degradation effect, the conventional inductor constraint is mathematically reformulated to redefine and expand the parameter feasible region of the inductor.
2. Frequency-Sweep-Based Resonance Point Evasion: To address the complex impedance coupling of the inverter-filter-cable-motor system, a comprehensive frequency sweep analysis is executed from the inverter output to the motor terminals. This enables precise identification of system resonance points, guiding the optimal capacitance selection (60 μF) to strategically shift the resonance frequencies away from vulnerable low-order harmonics.
3. Non-linear High-Frequency Thermal Reliability: Addressing the severe core losses under 4000 Hz carrier frequency excitation, a bidirectional iterative electromagnetic-thermal co-simulation scheme is implemented to guarantee the anti-saturation capability and thermal stability of the iron-silicon core under continuous forced air cooling.

By solving these overlapping constraints, this study provides a robust, boundary-explicit engineering framework for high-frequency motor protection under constrained operational environments.

2. Topology and Parameter Design of the LC Filter

2.1. Filter Structure Selection

The AC harmonic components generated by a PWM inverter are distributed in clusters around the carrier angular frequency and its integer multiples. As the carrier frequency increases, the entire harmonic spectrum shifts to a higher frequency band. Figure 1 shows the Fourier analysis results corresponding to the above conclusion. When the carrier frequency is 4000 Hz, the high-order harmonics are mainly distributed in the frequency range of 4000 Hz and its integer multiples. Consequently, a low-pass LC filter can effectively suppress these high-order harmonics [17,18].

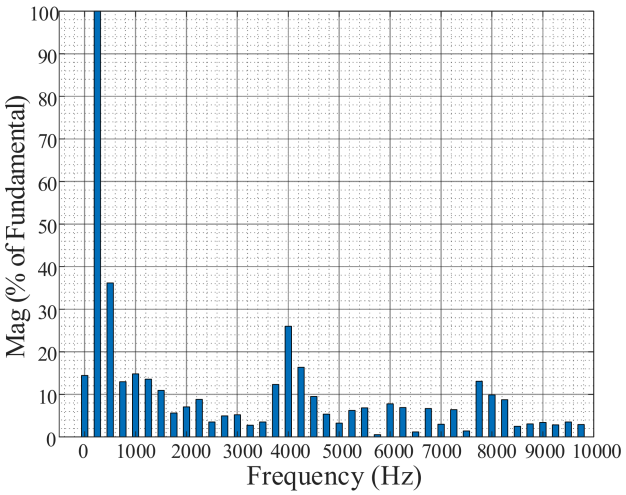


Figure 1. Frequency characteristic diagram of PWM wave output by the frequency converter.

For a three-phase LC filter, the capacitors can be arranged in either a star or delta configuration. The star connection imposes lower voltage withstand requirements on the capacitors. Additionally, it provides a neutral point that can be grounded, creating a low-impedance return path for common-mode interference currents. To maximize both voltage tolerance and common-mode noise suppression, we adopted the star-connected topology for this design. Its topology is shown in Figure 2.

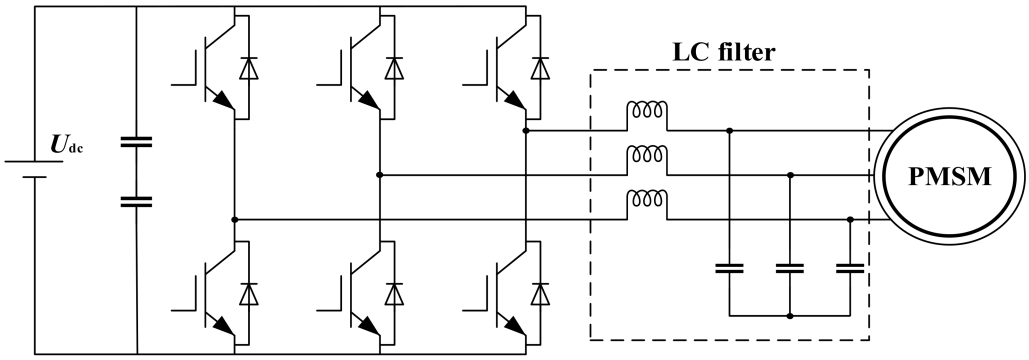


Figure 2. Three-phase LC passive filter topology (star connection).

2.2. Filter Parameter Design

We based the LC filter parameter design on a 15 kW mining submersible PMSM and its corresponding frequency converter. The relevant parameters of the adopted motor and frequency converter are listed in Table 2.

Table 2. Relevant Parameters of the Motor and Frequency Converter.

Motor and Frequency Converter Parameters	Value
Motor rated voltage	380 V
Motor rated current	22.8 A
Motor rated speed	5000 r/min
Fundamental frequency of PWM wave output by frequency converter	250 Hz
Carrier frequency of PWM wave output by frequency converter	4000 Hz

2.2.1. Cut-Off Frequency Range

Based on Figure 2, the transfer function of the LC filter is:

$$\frac{V_o}{V_i} = \frac{1}{s^2LC + 1} \tag{1}$$

In Equation (1), V_i denotes the input voltage of the sine-wave filter (inverter-side output voltage), and V_o represents the output voltage delivered to the remote motor terminals. The cut-off frequency f_{cut} is:

$$f_{cut} = \frac{1}{2\pi\sqrt{LC}} \tag{2}$$

According to Equation (2), the cut-off frequency of the filter depends only on the filter inductor L and filter capacitor C. In order to filter out high-order harmonics, its cut-off frequency should be much lower than the switching frequency f_c; at the same time, to avoid LC series resonance, its cut-off frequency should be higher than the fundamental frequency f_1 [19]. Therefore, the following formula should be satisfied when designing the LC sine filter:

$$2f_1 < \frac{1}{2\pi\sqrt{LC}} < \frac{1}{2}f_c \tag{3}$$

Therefore, the cut-off frequency range shall satisfy Equation (4):

$$500\ \text{Hz} \leq f_{\text{r}} \leq 2000\ \text{Hz} \tag{4}$$

2.2.2. Inductance Parameter Constraints

In the variable frequency speed regulation system, the inductance value is limited by the fundamental voltage drop. In order to avoid insufficient motor air gap flux and output torque to drive the load, this voltage drop must be controlled within a certain range when designing the LC filter [9]. Generally, the fundamental voltage drop of the filter inductor does not exceed 5% of the output voltage, that is:

$$U_{\text{d}} = 2\pi f L I_{\text{N}} \leq 0.05 U_{\text{N}} \tag{5}$$

In Equation (5), I_{N} and U_{N} represent the rated current and rated voltage of the motor, respectively. Considering the fundamental amplification effect, the amplitude (gain) of the transfer function of the LC filter to voltage at the fundamental frequency can be approximately expressed as:

$$Gain = \frac{1}{\left|1 - \left(\frac{f_1}{f_{\text{r}}}\right)^2\right|} \tag{6}$$

Assuming the cut-off frequency $f_{\text{cut}} = 1000$ Hz, substituting the two values into the formula gives:

$$Gain = \frac{1}{\left|1 - \left(\frac{250}{1000}\right)^2\right|} = \frac{1}{1 - 0.0625} = 1.0667 \tag{7}$$

Since the filter introduces a 6.67% voltage rise at 250 Hz, relaxing the allowable voltage drop of the inductor to 10% results in an actual motor terminal voltage drop of merely 3.33%. This value is well within the voltage regulation range of the converter DC bus (560 V). Therefore, the maximum allowable voltage drop is set to 10%, which satisfies Equation (8):

$$L \leq 0.6\ \text{mH} \tag{8}$$

Balancing the filtering efficacy against the voltage drop constraint, we selected an inductance value of 0.5 mH.

2.2.3. Capacitance Parameter Constraints

According to Equation (1), increasing the capacitance will decrease the cut-off frequency f_{cut} of the LC filter, thereby shifting the attenuation band toward lower frequencies and enabling more effective attenuation of harmonic components in higher frequency bands. However, as the motor stator windings act as an inductive load, they naturally form a higher-order LCL series structure with the filter inductor, filter capacitor, and the long cable. If the capacitance value is improperly selected, causing the resonance frequency of the LCL system to fall into the low-order harmonic bands of the 250 Hz fundamental frequency (such as the 3rd, 5th, or 7th harmonics), severe power quality deterioration and system stability issues will be induced.

To rigorously evaluate this, a simulation model of the long-distance variable-frequency drive system was established as shown in Figure 3. By performing a frequency sweep on the forward transmission characteristics of the entire system at the inverter output side, the resonance frequency points of the LCL network can be identified. Meanwhile, since the impedance characteristics of long cables heavily dictate the system's resonance distribution, a multi-stage lumped parameter equivalent circuit model, as illustrated in Figure 4, was utilized to simulate the 300 m cable. The core physical parameters (resistance, inductance,

and capacitance) used to construct this equivalent circuit model were extracted directly from the physical characteristics of the actual three-phase cable.

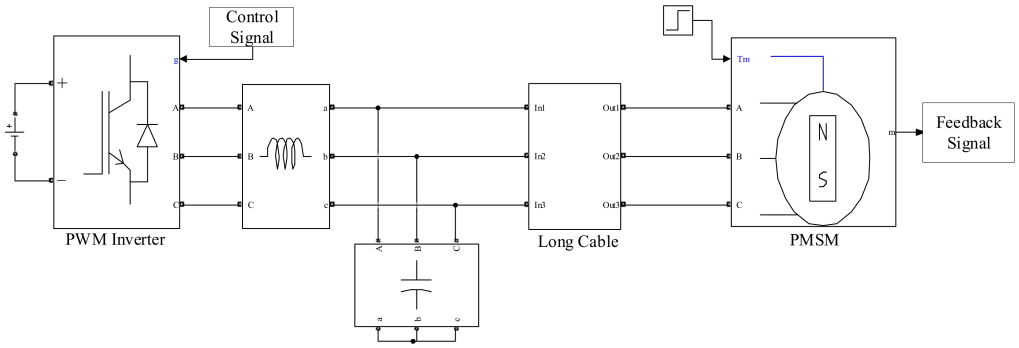


Figure 3. Simulation model of long-distance variable frequency drive system. In1, In2, and In3 represent the inputs of the long cable model, while Out1, Out2, and Out3 denote its outputs.

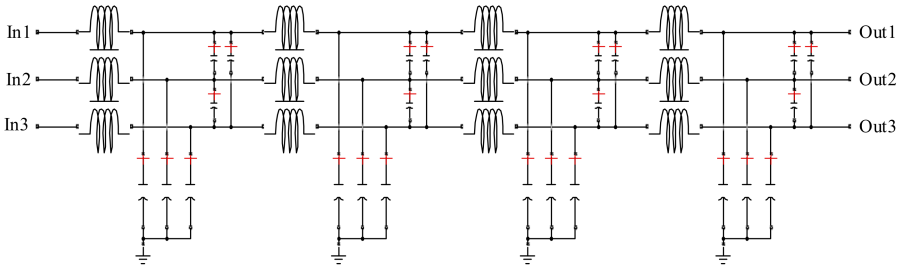


Figure 4. Multi-stage lumped parameter equivalent circuit model of the three-phase long cable.

The sweep results are shown in Figure 5. Frequency sweeps were performed for three different capacitance values. When the capacitance was 20 μF and 40 μF, the resonant peaks in the figure were located near 1750 Hz (the 7th harmonic) and 1250 Hz (the 5th harmonic). When the capacitance is optimized at 60 μF, the coupled system's resonant frequency is shifted to approximately 1000 Hz.

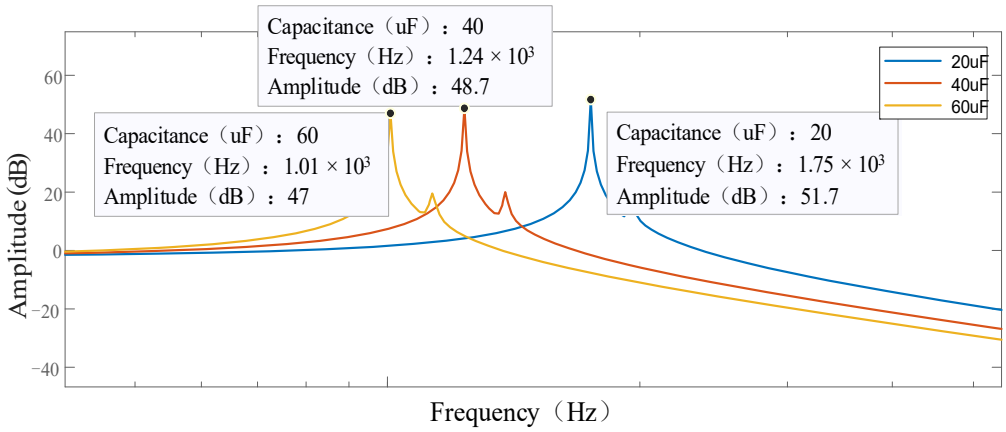


Figure 5. Amplitude-frequency characteristic diagram of forward transmission characteristics.

For a 250 Hz fundamental frequency drive system, the characteristic harmonic energy of the PWM wave is predominantly concentrated on odd-order harmonics, specifically manifested as the 3rd harmonic (750 Hz) and the 5th harmonic (1250 Hz). Although a minor amount of even-order harmonic components may exist due to the non-ideal PWM wave output from the inverter (e.g., the 4th harmonic at 1000 Hz), their energy levels are negligible compared to the dominant odd-order harmonics. By strategically positioning

the undamped system resonance peak exactly at 1000 Hz—the midpoint energy trough between the 3rd and 5th harmonics—the resonance point successfully avoids the frequency bands of high-energy characteristic excitations. At the critical odd-harmonic frequencies, the transmission gain remains sufficiently suppressed, offering a robust safety margin.

3. Component Selection and Systemic Risk Analysis

3.1. Magnetic Core Anti-Saturation Design

Saturation resistance is particularly critical in the application scenario of this design. During motor startup, the current output by the frequency converter includes not only the motor's own starting current but also the instantaneous surge from charging the filter capacitor. The superposition of these two components results in a peak starting current far exceeding the rated operating value, which is typically estimated to be approximately 1.5 to 3.0 times the rated continuous current in practical drive systems. If the magnetic core exhibits insufficient saturation resistance, the inductor will instantly enter saturation, causing a sharp drop in inductance. This not only fails to suppress current spikes but may also exacerbate current surges or even lead to short circuits [20,21].

To prevent this, we selected a Magnetics XFlux (Iron-Silicon Alloy) powder core (Magnetics, Pittsburgh, PA, USA) with an initial permeability of 26. This material provides exceptional anti-saturation properties. Furthermore, we specified a wire diameter rated for 50 A to reserve sufficient current-carrying margin, thereby minimizing copper losses and thermal rise. The designed inductor is shown in Figure 6.

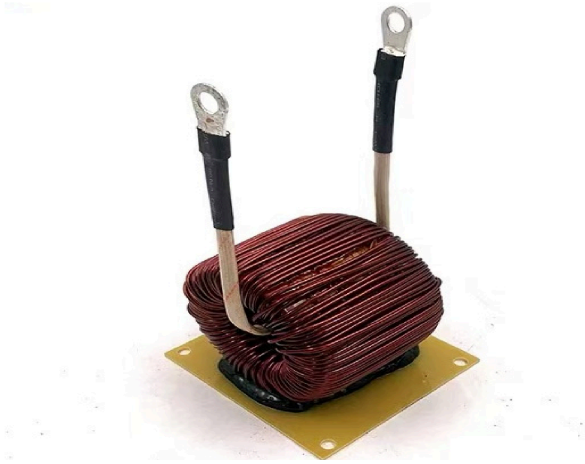


Figure 6. The physical image of the 0.5 mH inductor.

3.2. Electromagnetic-Thermal Co-Simulation

In long-cable systems, the inductor operates continuously under high-frequency PWM excitation [22,23]. To accurately evaluate the loss characteristics and thermal reliability of the filter inductor under high-frequency PWM operating conditions, a co-simulation scheme combining Maxwell 3D (version 2024 R1) electromagnetic simulation and Icepak (version 2024 R1) thermal field simulation is adopted [20]. The scheme completes inductor loss calculation and steady-state temperature solution under forced air cooling conditions, verifying whether the selected iron-silicon powder core inductor meets the requirements for long-term safe operation [24].

Taking the 0.5 mH iron-silicon powder core filter inductor designed in this paper as the research object, a 1:1 three-dimensional simulation model including the magnetic core, windings and external air domain is established in Maxwell 3D, as shown in Figure 7.

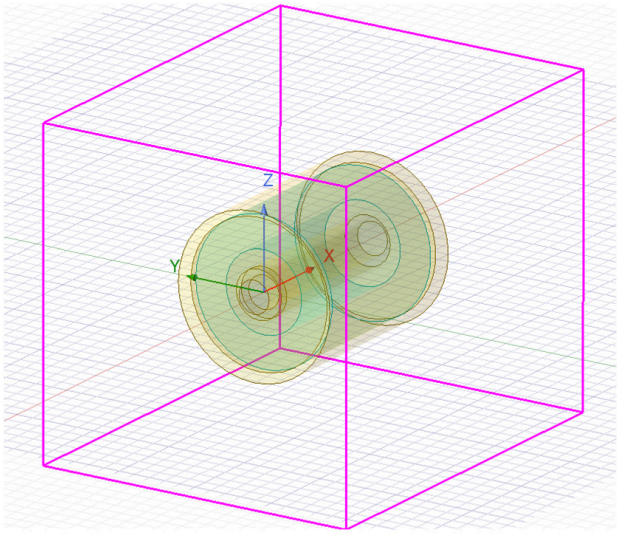


Figure 7. Simulation model of inductor thermal losses, where the green body represents the magnetic core, the yellow body denotes the coil, and the pink box indicates the solution domain.

Material parameters are defined strictly in accordance with the actual prototype. The winding is set as pure copper, while the B-H magnetization curve and B-P core loss density curve officially provided by Magnetics are imported for the magnetic core material, as illustrated in Figure 8.

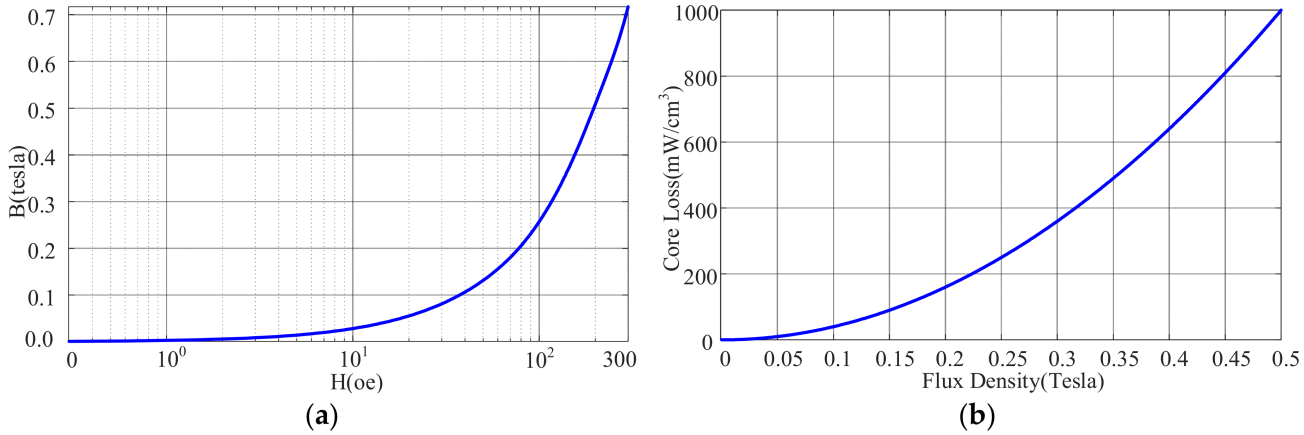


Figure 8. Magnetic core material parameter curves: (**a**) B-H curve (magnetization curve); (**b**) B-P curve (core loss density curve).

The excitation applied to the inductive components was set to an alternating current with an RMS value of 26.5 A at a frequency of 4000 Hz, which perfectly aligns with the system's carrier/switching frequency (f_c).

Icepak receives the loss heat source data exported from Maxwell. Meanwhile, the real-time calculated temperature field is fed back to Maxwell to revise temperature-dependent electromagnetic parameters such as the B-H curve and electrical conductivity of the core material, as shown in Figure 9. Accordingly, bidirectional iterative coupling between the electromagnetic field and temperature field is realized, which can better reflect the actual operating state.

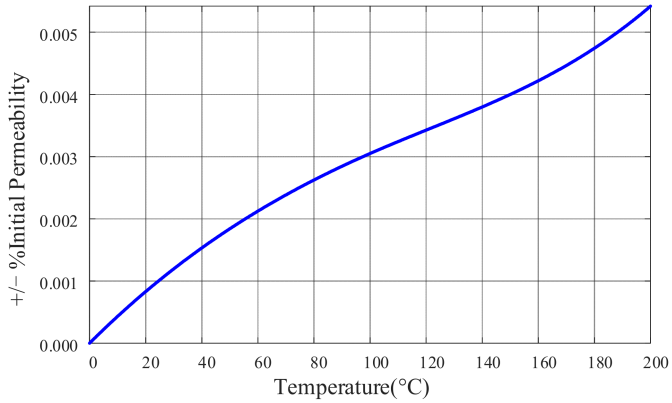
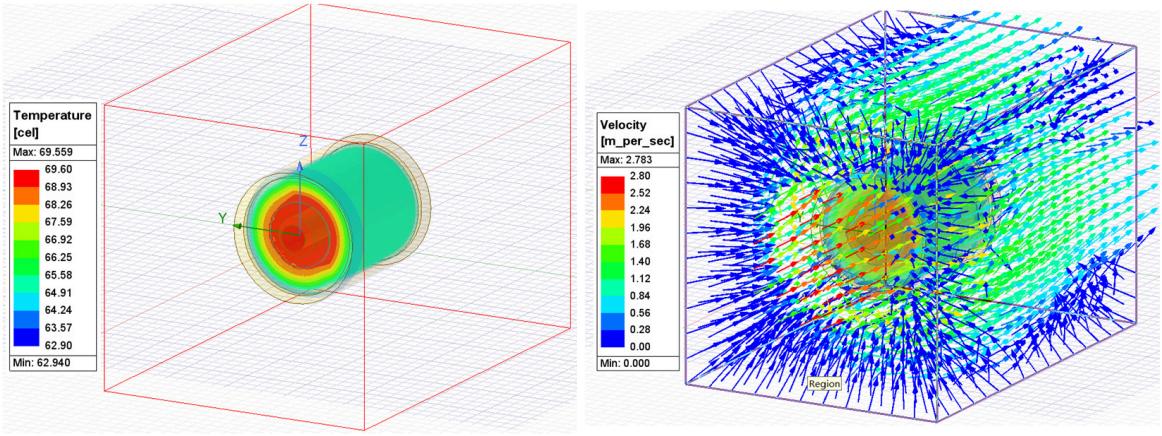


Figure 9. Variation of temperature correction coefficient with temperature.

For the meshing strategy, an adaptive grid refinement technique with an automatic tetrahedral mesh generation is employed to balance computational efficiency and solution resolution. In terms of the solution domain and boundary conditions, an air box enclosing the inductor model is established as the ultimate computational domain, with open boundary conditions assigned to simulate a free convective environment. Additionally, forced-air cooling is adopted with a cooling fan airflow of 50 cubic feet per minute (CFM). The inlet wind speed, an ambient temperature of 25 °C, and natural convection heat transfer coefficients are precisely configured to replicate the actual hardware installation and heat exchange boundaries.

The thermal simulation results are presented in Figure 10. Under forced air cooling with an airflow of 50 CFM, the maximum steady-state temperature of the inductor is 69 °C. Hot spots are located at the core center and the inner side of windings, with an overall uniform temperature distribution and no local overheating.



(**a**) (**b**)

Figure 10. Simulation results: (**a**) Steady-state temperature distribution; (**b**) Flow velocity vector diagram.

The co-simulation results verify that the adopted filter inductor possesses reasonable core loss under rated conditions. Both power loss and temperature rise comply with the design specifications, which ensures the thermal reliability and long-term operational stability of the long-distance variable-frequency drive system under continuous operation.

3.3. Self-Excited Oscillation Risk Assessment

When a variable frequency drive system fails, the trigger pulses of switching tubes are generally blocked to protect power devices. If the inverter shuts down abruptly while the motor rotor continues rotating due to inertia, the filter capacitor supplies capacitive current

to the motor stator. This places the motor in a self-excited generating state and triggers self-oscillation between the filter capacitor and the motor. Once self-excitation occurs, the amplitudes of the self-excited current and motor terminal voltage continuously increase. With the rising self-excited current, the motor magnetic circuit becomes saturated, and the terminal voltage reaches its peak value. Afterwards, the rotational speed gradually decreases, and the terminal voltage eventually drops to zero.

Figure 11 presents the capacitance characteristic curve and the motor no-load characteristic curve. The intersection of the two curves determines the maximum self-excited voltage. A smaller filter capacitance leads to a larger slope of the capacitance curve and a lower self-excited voltage.

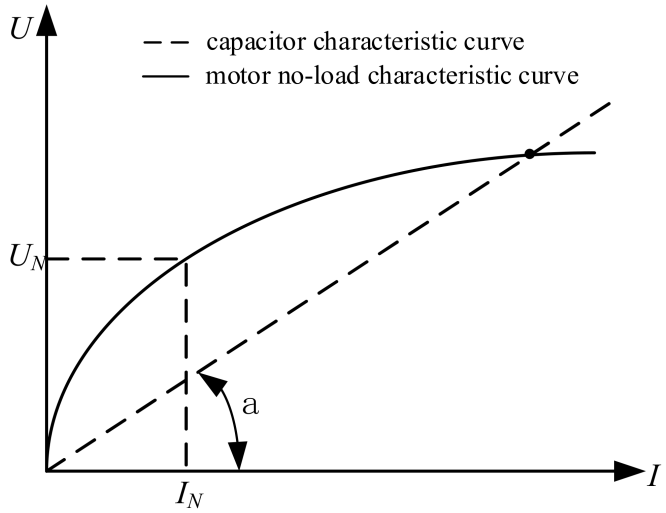


Figure 11. No-load characteristic curve of the motor and capacitance characteristic curve.

It should be emphasized that the assessment of self-excited oscillation risk is not incorporated as a constraint within the core parameter design procedure, primarily owing to the hyper-complex, non-linear electromagnetic evolution and varying rotor deceleration that make precise analytical derivation mathematically intractable. Instead, this analysis serves as a critical post-design verification phase to evaluate the boundary safety of the already determined filter parameters. To pragmatically quantify this dynamic behavior in lieu of complex mathematical approximations, the system's transient response under emergency conditions is evaluated directly through empirical testing in the following section.

4. Experimental Validation and Results

To verify the effect of the LC filter on suppressing motor terminal overvoltage and improving power quality, a counter-dragging experimental platform simulating variable frequency drive with long cables is built. The structure of the platform is shown in Figure 12. Notably, a 20 m cable was used for the hardware prototype due to laboratory space and safety constraints, while a 300 m cable was evaluated in simulations. Although transient overvoltage is cable-length dependent, its mitigation relies fundamentally on eliminating high dv/dt pulses at the inverter output. By restoring a smooth sinusoidal source, the prerequisite for traveling wave reflection is removed. Thus, verifying the wave-shaping capability on a 20 m platform provides sufficient equivalent validation for the 300 m system, as removing high dv/dt pulses prevents reflection-induced overvoltage regardless of cable length.

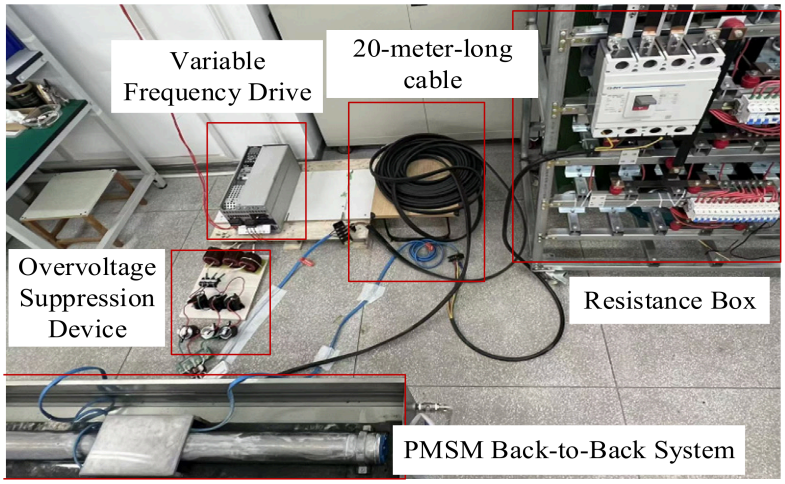


Figure 12. Schematic diagram of the experimental platform.

Finally, under constant-torque operation of the motor, the voltage and current waveforms at the motor terminal before and after filter installation are shown in Figures 13 and 14, respectively. The comparative data are listed in Table 3.

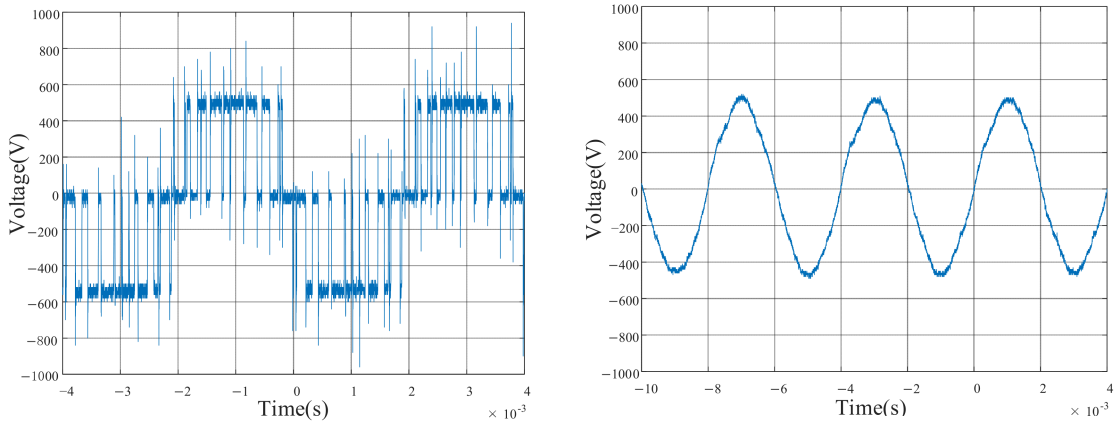


Figure 13. (**a**) Line voltage waveform at motor terminals before filter installation; (**b**) Line voltage waveform at motor terminals after filter installation.

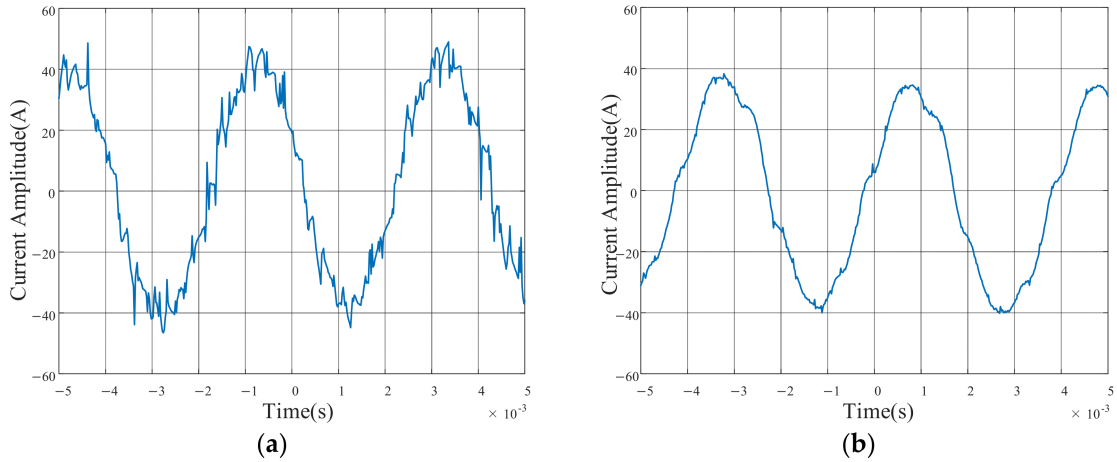


Figure 14. (**a**) Line current waveform at motor terminals without the filter; (**b**) Line current waveform at motor terminals with the filter.

Table 3. Data Comparison Before and After Filter Installation.

	Maximum Peak Voltage at Motor Terminals (V)	Total Harmonic Distortion
Before Filter Installation	900	37.23%
After Filter Installation	505	4.64%

Without the filter, the measured voltage waveforms exhibited severe PWM reflection at the motor terminals. The peak line voltage exceeded 900 V (THD = 37.23%), and the current waveform contained a high density of high-order harmonics, posing a severe threat to stator insulation. After installing the designed 0.5 mH/60 μF LC filter at the inverter output, the terminal waveforms transitioned to smooth sinusoids. The peak terminal voltage dropped to a safe 505 V, entirely eliminating the dangerous transient spikes. Concurrently, the total harmonic distortion was reduced to 4.64%, where the FFT analysis confirmed that the lower-order characteristic harmonics were attenuated to a negligible level, and the high-frequency switching harmonics around 4000 Hz were thoroughly flattened to virtually zero. These experimental results confirm that the filter successfully mitigates overvoltage and restores power quality without degrading fundamental motor performance.

Furthermore, under the same forced-air cooling conditions as the simulation, the inductor temperature basically stabilized at 60 °C after 3 h of operation, verifying its thermal stability.

To complete the post-design safety check regarding the self-excited oscillation risk declared in Section 3.3, we systematically conducted a sudden power-off experiment under rated high-speed conditions. As shown in Figure 15, the transient terminal voltage waveform captured immediately following the interruption reveals a self-excited resonant oscillation with a maximum instantaneous peak of approximately 800 V. Crucially, due to the high-bandwidth damping attributes of the system and the rapid deceleration of the pump rotor, we observed that this 800 V oscillation attenuates heavily within an exceptionally brief duration. Compared to the continuous degradation caused by long-cable steady-state traveling wave overvoltages (which continuously subject the motor insulation to nearly 900 V spikes without the filter), this short-lived, millisecond-level transient disturbance imposes negligible thermal and dielectric hazards to the motor stator winding insulation. This empirical validation robustly confirms that our final filter parameters maintain an excellent safety margin under real-world emergency conditions.

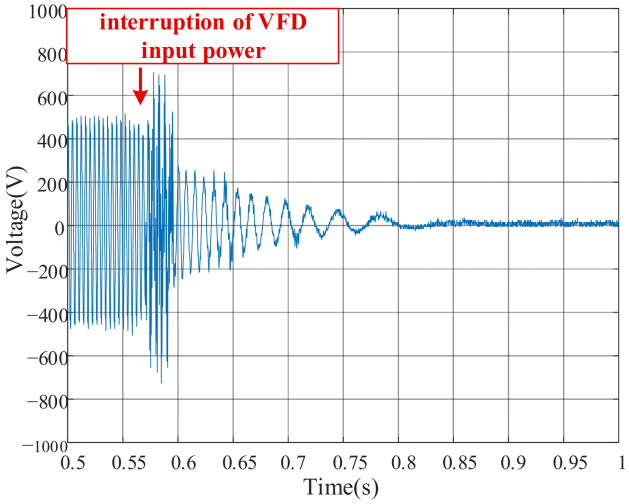


Figure 15. Behavior of motor terminal voltage during sudden interruption of VFD input power.

To further justify the general applicability and reliability of the proposed filter under potential variations in operating conditions, the system's electrical immunity is evaluated from a wave propagation perspective. In long-cable drive systems, the transient motor-terminal overvoltage is governed by traveling wave reflection, which is strictly driven by the steep rising edges (high dv/dt) of the inverter's PWM voltage pulses. Crucially, the motor's low-frequency operational conditions—such as load torques, speeds, and thermal states—alter the fundamental current magnitudes or operating frequencies but do not affect the intrinsic switching rise times of the inverter. Since the primary mechanism of overvoltage suppression relies entirely on the filter's capability to eliminate these high-dv/dt voltage pulses right at the inverter output, restoring a smooth sinusoidal source inherently removes the prerequisite for traveling wave reflections. Consequently, verifying the filter's wave-shaping performance under the rated steady-state condition provides sufficient validation, as the eradication of steep rising edges guarantees robust overvoltage suppression regardless of downstream mechanical or thermal load variations.

5. Conclusions

This study addresses the critical challenge of transient overvoltage induced by traveling wave reflection in long-cable, high-frequency (250 Hz) PMSM drives used in deep-well mining. Acknowledging the severe spatial constraints at the motor terminal, we developed an inverter-side passive LC filter design and optimization methodology. The primary findings are:

1. By integrating constraints across the resonant frequency range, fundamental voltage drop, and low-order harmonic avoidance, we established optimal filter parameters (0.5 mH and 60 μF). This configuration successfully balances high-frequency attenuation with fundamental transmission efficiency.
2. The selection of an iron-silicon alloy powder core prevents saturation failure during the high-current startup phase. Coupled with electromagnetic-thermal validation, the design guarantees long-term thermal stability under continuous forced air cooling.
3. Finally, experimental validation confirms the system's efficacy. The implemented filter safely reduces peak terminal overvoltage from 900 V to 505 V and suppresses THD to below 5%.

This methodology provides a reproducible, highly reliable technical solution for overvoltage protection in high-frequency motor drives subjected to long-cable transmission and constrained installation environments.

Author Contributions: Conceptualization, G.Z. (Genmao Zhou) and Y.D.; methodology, Y.T., L.C. and G.Y.; validation, Z.D. and G.Z. (Gang Zhang); formal analysis, Z.D. and G.Z. (Gang Zhang); investigation, G.Z. (Genmao Zhou) and Y.T.; resources, Y.D. and L.C.; data curation, Z.D. and G.Y.; writing—original draft preparation, Z.D. All authors have read and agreed to the published version of the manuscript.

Funding: This research was funded by the first author's institution under the project "Power quality evaluation and motor-end overvoltage suppression technology application for variable frequency drive system of submersible pumps in in-situ leaching uranium mining", grant number [2025YFY1]. The APC was funded by the same project.

Data Availability Statement: The original contributions presented in this study are included in the article. Further inquiries can be directed to the corresponding author.

Conflicts of Interest: Authors Genmao Zhou, Yinquan Ding, Yiwei Tang, Li Chen and Guohui Yang were employed by the company Xinjiang CNNC Tianshan Uranium Industry Co., Ltd. The remaining authors declare that the research was conducted in the absence of any commercial or financial relationships that could be construed as a potential conflict of interest.

Abbreviations

The following abbreviations are used in this manuscript:

PMSM	Permanent Magnet Synchronous Motor
PWM	Pulse Width Modulation
THD	Total Harmonic Distortion

References

1. Chen, Y.; Zang, B.; Wang, H.; Liu, H.; Li, H. Composite PM Rotor Design and Alternating Flux Density Harmonic Component Analysis of a 200 kW High-Speed PMSM Used in FESS. *IEEE Trans. Ind. Appl.* **2023**, *59*, 1469–1480. [CrossRef]
2. Wang, Q.; Zhao, X.; Yang, P.; Hua, W.; Buja, G. Effects of Triangular Wave Injection and Current Differential Terms on Multiparameter Identification for PMSM. *IEEE Trans. Power Electron.* **2024**, *39*, 2943–2947. [CrossRef]
3. Sadoughi, M.; Fateh, F.; Mirafzal, B. Overvoltage Stress on AC Motor Winding Insulations Driven by Fast-Switching Inverters: A Study. In Proceedings of the 2024 IEEE Kansas Power and Energy Conference (KPEC), Manhattan, KS, USA, 25–26 April 2024; pp. 1–6.
4. Dorn-Gomba, L.; Ramoul, J.; Reimers, J.; Emadi, A. Power Electronic Converters in Electric Aircraft: Current Status, Challenges, and Emerging Technologies. *IEEE Trans. Transp. Electrif.* **2020**, *6*, 1648–1664. [CrossRef]
5. de Paula, V.C.; de Paula, H. Employing DC Transmission in Long Distance AC Motor Drives: Analysis of the Copper Economy and Power Losses Reduction in Mining Facilities. In Proceedings of the 2015 IEEE Industry Applications Society Annual Meeting, Addison, TX, USA, 18–22 October 2015; pp. 1–7.
6. Dzhankhotov, V.; Pyrhönen, J. Passive LC Filter Design Considerations for Motor Applications. *IEEE Trans. Ind. Electron.* **2013**, *60*, 4253–4259. [CrossRef]
7. Smochek, M.; Pollice, A.F.; Rastogi, M.; Harshman, M. Long Cable Applications From a Medium-Voltage Drives Perspective. *IEEE Trans. Ind. Appl.* **2016**, *52*, 645–652. [CrossRef]
8. Tilea, I.; Munteanu, C. Motor Cable Electric Parameter Effects on the Overvoltage Phenomenon in Inverter Driven Motors. In Proceedings of the 2013 8th International Symposium on Advanced Topics in Electrical Engineering (ATEE), Bucharest, Romania, 23–25 May 2013; pp. 1–6.
9. Hanigovszki, N.; Landkildehus, J.; Blaabjerg, F. Output Filters for AC Adjustable Speed Drives. In Proceedings of the APEC 07—Twenty-Second Annual IEEE Applied Power Electronics Conference and Exposition, Anaheim, CA, USA, 25 February–1 March 2007; pp. 236–242.
10. Choochuan, C. A Survey of Output Filter Topologies to Minimize the Impact of PWM Inverter Waveforms on Three-Phase AC Induction Motors. In Proceedings of the 2005 International Power Engineering Conference, Singapore, 29 November–2 December 2005; pp. 1–544.
11. Lee, S.; Nam, K. Overvoltage Suppression Filter Design Methods Based on Voltage Reflection Theory. *IEEE Trans. Power Electron.* **2004**, *19*, 264–271. [CrossRef]
12. Steinke, J.K. Use of an LC Filter to Achieve a Motor-Friendly Performance of the PWM Voltage Source Inverter. *IEEE Trans. Energy Convers.* **1999**, *14*, 649–654. [CrossRef]
13. Mishra, P.; Maheshwari, R. Design, Analysis, and Impacts of Sinusoidal LC Filter on Pulsewidth Modulated Inverter Fed-Induction Motor Drive. *IEEE Trans. Ind. Electron.* **2020**, *67*, 2678–2688. [CrossRef]
14. Wu, X.; Ji, Y.; Li, C.; Xu, Y.; Zou, J.; Tian, L.; Chen, S.; Ma, Z.; Han, Y. Review and New Expansion of the Active Damping Strategy of the PMSM Drive System with LC Sine Wave Filter. *CES Trans. Electr. Mach. Syst.* **2025**, *9*, 268–288. [CrossRef]
15. Li, C.; Xu, Y.; Zou, J.; Zhang, W.; Li, S.; Chen, S.; Ma, Z.; Wu, X. Sensorless Control of LC-Filtered PMSM Drives Using an Easy-Tuning Full-Order Flux Observer. *IEEE Trans. Ind. Electron.* **2026**, 1–12. [CrossRef]
16. Wu, X.; Li, C.; Zhang, Y.; Chen, S.; Ma, Z.; Han, Y.; Zhang, X.; Tan, G. Sensorless Control of IPMSM Equipped With LC Sinusoidal Filter Based on Full-Order Sliding Mode Observer and Feedforward QPLL. *IEEE Trans. Power Electron.* **2024**, *39*, 8072–8085. [CrossRef]
17. Jiang, Y.; Wu, W.; He, Y.; Chung, H.S.-H.; Blaabjerg, F. New Passive Filter Design Method for Overvoltage Suppression and Bearing Currents Mitigation in a Long Cable Based PWM Inverter-Fed Motor Drive System. *IEEE Trans. Power Electron.* **2017**, *32*, 7882–7893. [CrossRef]
18. He, J.; Sizov, G.Y.; Zhang, P.; Demerdash, N.A.O. A Review of Mitigation Methods for Overvoltage in Long-Cable-Fed PWM AC Drives. In Proceedings of the 2011 IEEE Energy Conversion Congress and Exposition, Phoenix, AZ, USA, 17–22 September 2011; pp. 2160–2166.
19. Stubenrauch, F.; Seliger, N.; Schmitt-Landsiedel, D. Design and Performance of a 200 kHz GaN Motor Inverter with Sine Wave Filter. In Proceedings of the PCIM Europe 2017, International Exhibition and Conference for Power Electronics, Intelligent Motion, Renewable Energy and Energy Management, Nuremberg, Germany, 16–18 May 2017; pp. 1–9.

20. Vitale, G.; Lullo, G.; Scirè, D. Thermal Stability of a DC/DC Converter With Inductor in Partial Saturation. *IEEE Trans. Ind. Electron.* **2021**, *68*, 7985–7995. [CrossRef]
21. Ojeda-Rodríguez, Á.; Cano-Gómez, G.; Bernal-Méndez, J. Analysis and Modelling of a Ring Core Inductor under Saturation Effect. In Proceedings of the 2023 International Symposium on Electromagnetic Compatibility—EMC Europe, Krakow, Poland, 4–8 September 2023; pp. 1–6.
22. Li, Z.; Han, W.; Xin, Z.; Liu, Q.; Chen, J.; Loh, P.C. A Review of Magnetic Core Materials, Core Loss Modeling and Measurements in High-Power High-Frequency Transformers. *CPSS Trans. Power Electron. Appl.* **2022**, *7*, 359–373. [CrossRef]
23. Mu, M.; Li, Q.; Gilham, D.J.; Lee, F.C.; Ngo, K.D.T. New Core Loss Measurement Method for High-Frequency Magnetic Materials. *IEEE Trans. Power Electron.* **2014**, *29*, 4374–4381. [CrossRef]
24. Swihart, M.A. Inductor Cores–Material and Shape Choices. Magnetics. 2004. Available online: https://www.mag-inc.com (accessed on 8 June 2026).

Disclaimer/Publisher's Note: The statements, opinions and data contained in all publications are solely those of the individual author(s) and contributor(s) and not of MDPI and/or the editor(s). MDPI and/or the editor(s) disclaim responsibility for any injury to people or property resulting from any ideas, methods, instructions or products referred to in the content.